THE JOURNAL OF PHYSICAL CHEMISTRY LETTERS
A JOURNAL OF THE AMERICAN CHEMICAL SOCIETY

pubs.acs.org/JPCL Letter

Observation of Competitive Nonadiabatic Photodissociation Dynamics of H_2S^+ Cations

Zhiwen Luan, Yanlin Fu, Yuxin Tan, Yaling Wang, Baokun Shan, Jie Li, Xiaoguo Zhou,* Wentao Chen, Lijie Liu, Bina Fu,* Dong H. Zhang, Xueming Yang, and Xingan Wang*

Cite This: J. Phys. Chem. Lett. 2022, 13, 8157−8162 Read Online

ACCESS | Metrics & More | Article Recommendations | Supporting Information

ABSTRACT: A comprehensive understanding of dissociation mechanisms is of fundamental importance in the photochemistry of small molecules. Here, we investigated the detailed photodissociation dynamics of H_2S^+ near 337 nm by using the velocity map ion imaging technique together with the theoretical characterizations by developing global full-dimensional potential energy surfaces (PESs). Rotational state resolved images were acquired for the $S^+(^4S)$ + H_2 product channel. Significant changes in product total kinetic energy release distributions and angular distributions have been observed within a small excitation photon energy range of 5 wavenumbers. Analysis based on the full-dimensional PESs reveals that two nonadiabatic pathways determined by the transition state connecting two minima on the $1^2A'$ state are responsible for the dramatic variation of observed product distributions. The current study has directly witnessed the competitive photodissociation mechanisms controlled by a critical energy point on the PES, thereby providing in-depth insight into the nonadiabatic dynamics in photochemistry.

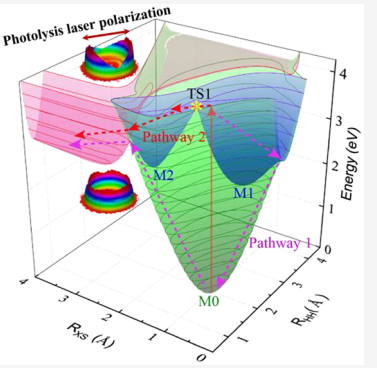

Nonadiabatic phenomenon widely exists in the photodissociation of molecules due to increasingly stronger electronic degeneracies in exited quantum states.[1] Through electronic degeneracies, nonadiabatic effects can not only influence the overall product channels but also affect the exact dynamics, such as branching ratios and angular distributions.[2] As a result, high-resolution observation and accurate characterization of nonadiabatic effects are indispensable in elucidating photodissociation dynamics in highly excited states. Hydrogen sulfide cation (H_2S^+) is a key component and an essential partaker in the synthesis of sulfur-containing molecules in various environments.[3−5] As a prototype of bent triatomic ions, H_2S^+ shows nonadiabatic couplings between the excited states.[6−8] Furthermore, the photodissociation of hydrogen sulfide cations $H_2S^+(X^2B_1) \rightarrow H_2(X^1\Sigma_g^+)+S^+(^4S)$ is a spin-forbidden process and can only take place via nonadiabatic couplings.[9] Over the past decades, much attention has been made to experimental and theoretical studies of H_2S^+ in an effort to clarify the photodissociation dynamics.[10−20]

The experimental studies of the H_2S^+ can be traced back to the 1970s. Horani et al. first observed the emission spectrum of H_2S^+ in the range of 400 nm-600 nm.[21] Based on this spectrum, Dixon et al. verified that there is a barrier to the linear geometry of approximately 4600 cm^{-1} by comparing the photoelectron spectrum of H_2S^+ as well as presenting the transition selection rules for the photoelectron spectra.[21] Duxbury et al. then discovered the topological natures of the X^2B_1 and A^2A_1 states of H_2S^+ and illustrated the convoluted rovibronic structure of the excited states involving both the Renner-Teller effect and spin−orbit coupling.[22] Ng and co-workers presented the photoelectron spectrum of H_2S with the upgraded spectral resolution using the pulsed-field ionization technique combined with the vacuum ultraviolet synchrotron radiation source, providing the quantitatively refined data for the vibronic term values associated with the photoionization processes that produce H_2S^+ in different electronic states of X^2B_1, A^2A_1, or B^2B_2.[23] Ashfold and colleagues then reported the velocity map ion imaging results of the photodissociation of H_2S^+ that reveal the unique role of nuclear spin on the photodissociation; the Renner-Teller coupling and spin−orbit coupling have also been found to play an important role in the dissociation process.[24,25] In 2014, Duxbury et al. combined various types of spectroscopies to present a detailed description of the Renner-Teller effect in the A^2A_1 and X^2B_1 of H_2S^+.[26] The theoretical investigation of H_2S^+ was mainly focused on stationary-point electronic structure calculations for the lowest several electronic states and/or two-dimensional potential energy curves with one degree of freedom fixed at a specific value. The early study of Hirsch and Bruna[27] presented a correlation diagram with dissociation products for the X^2B_1, A^2A_1, and B^2B_2 states of H_2S^+. Hirst proposed a possible pathway of $S^+(^4S)$ formation from the A^2A_1 state and analyzed

Received: June 18, 2022
Accepted: August 16, 2022

https://doi.org/10.1021/acs.jpclett.2c01892
J. Phys. Chem. Lett. 2022, 13, 8157−8162

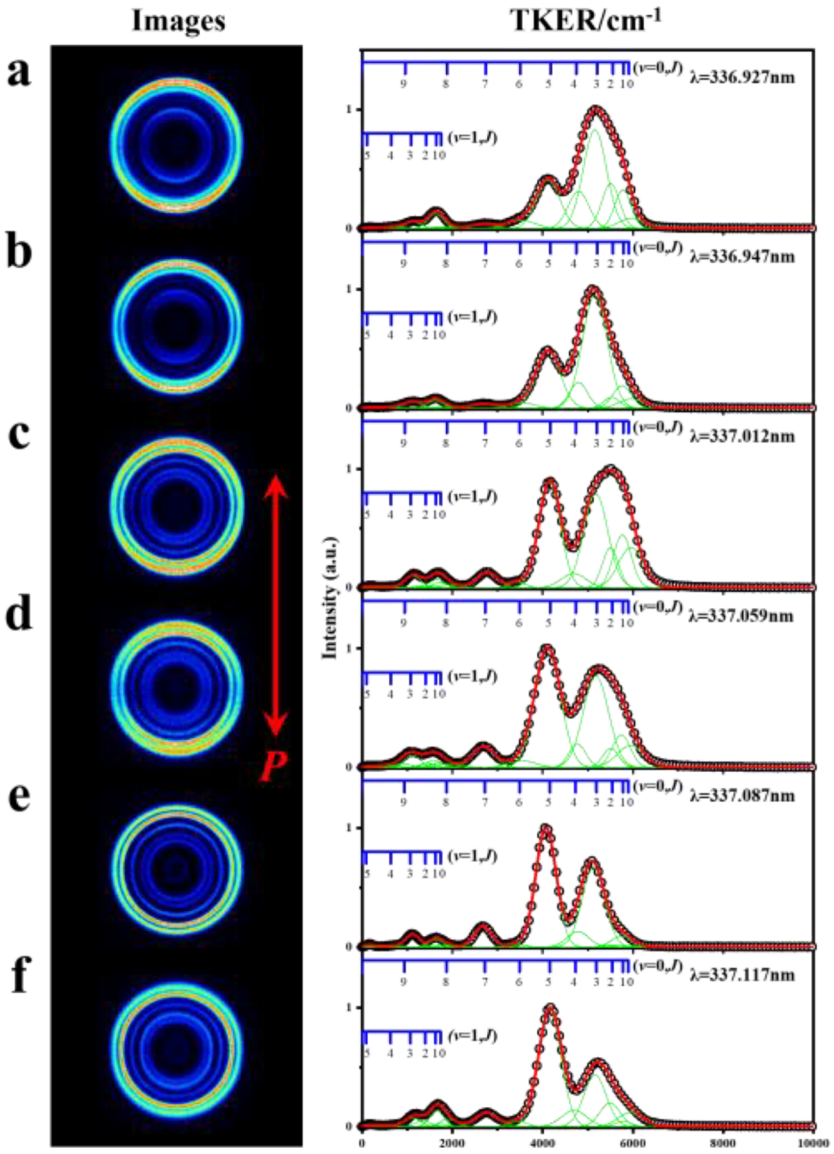

Figure 1. Ion images and total kinetic energy release (TKER) distributions (arb. units) of $S^+(^4S)$ products from the photodissociation of $H_2S^+(X^2B_1)$ at wavelengths (a) 336.927 nm, (b) 336.947 nm, (c) 337.012 nm, (d) 337.059 nm, (e) 337.087 nm, and (f) 337.117 nm. The rings shown in the images correspond to the rovibrational state of the $H_2(X^1\Sigma_g^+)$ coproducts.

the conical intersection between A^2A_1 and the higher B^2B_2 state by performing multireference configuration interaction calculations.[28] In 2005, Huang and co-workers optimized the stationary points and analyzed the minimum energy curves of $1^2A''$, $1^2A'$, and $2^2A'$ states by CASPT2 calculations.[29] They further investigated the potential energy curves of S-loss and H-loss, which reveals that the $1^2A''$ and $1^2A'$ states correlate with $H_2 + S^+(^2D)$, while the $1^4A''$ state correlates with $H_2 + S^+(^4S)$.[30] Possible dissociation mechanisms of S-loss and H-loss from the A state were also explored based on reduced-dimensional potential energy curves.

Previous studies have shown that nonadiabatic effects, such as Renner-Teller coupling and spin−orbit coupling, play a vital role during the photodissociation process. Yet, the detailed dynamics information and the underlying mechanism for the photodissociation over critical energies that involve nonadiabatic effects remain unclear. Here, we conducted synergistic experimental and theoretical research on the photodissociation of H_2S^+ to produce H_2 and S^+ fragments in order to reveal the detailed dynamics information and the underlying mechanism for the photodissociation over critical energies. A high-resolution experiment combined with high-level theoretical characterizations was applied to clearly illustrate the nonadiabatic dynamics in this work. The experiments were carried out using a time-sliced velocity map ion imaging apparatus with high energy and angular resolution which has been described in the Supporting Information. By detecting the ion images of S^+ photofragments, a remarkable variation has been observed in the translational energy distributions and angular distributions at different photodissociation wavelengths in a very limited energy region. Full-dimensional potential energy surfaces (PESs) of $X^2B_1(1^2A'')$, $A^2A_1(1^2A')$, and $1^4A_2(1^4A'')$ states were developed by the fundamental invariant-neural network (FI-NN) approach[31,32] based on extensive multireference configuration interaction (MRCI) calculations. The theoretical analysis based on the PESs reveals two possible pathways depending on the excitation energy, which were mainly

https://doi.org/10.1021/acs.jpclett.2c01892
J. Phys. Chem. Lett. 2022, 13, 8157−8162

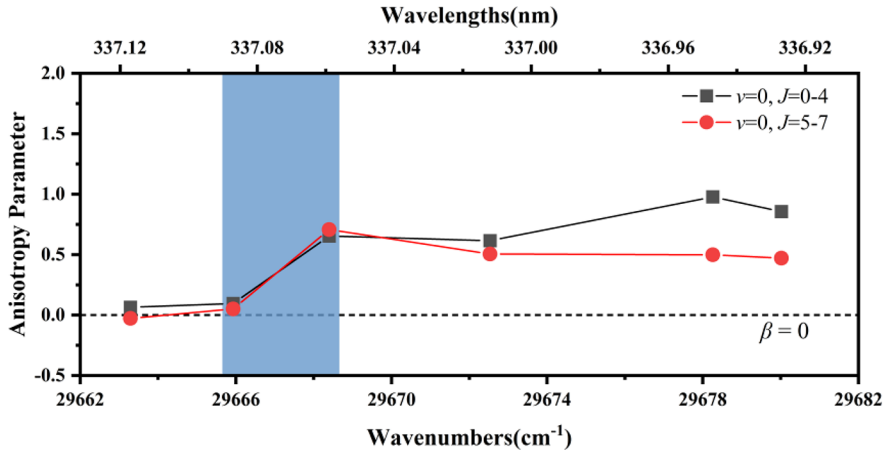

Figure 2. Anisotropy parameters (β values) for rovibrational states of the $H_2(X^1\Sigma_g^+)$ product as a function of the photodissociation wavenumbers between 29663 and 29680 cm^{-1}.

controlled by the transition state (TS) connecting two minima on the $1^2A'$ state, thereby providing a reasonable interpretation of experimental results.

The H_2S^+ parent cations were prepared by 2 + 1 resonance-enhanced multiphoton ionization (REMPI) of the jet-cooled H_2S via the strong Q branch of the $^1A_1$-X^1A_1 two photon resonances at a wavelength of about 302.6 nm which includes both ortho and para nuclear spin symmetry. The images of the S^+ products from H_2S^+ photodissociation $H_2S^+(X^2B_1) \rightarrow H_2(X^1\Sigma_g^+) + S^+(^4S)$ were measured at six photodissociation wavelengths, namely, 336.927, 336.947, 337.012, 337.059, 337.087, and 337.117 nm. These particular wavelengths correspond to the six adjacent local maxima in the S^+ signal intensity. Based on previous photoelectron spectroscopy studies,[23] these photodissociation wavelengths correspond to the vibration−rotation level identified as $A^2A_1(0,12,0)$ $K = 1$.

The noise of the experiment mainly came from the photoionization laser beam, so the pulse energies of the photoionization laser were controlled at a low power density to optimize the signal-to-noise. The background of all images was taken with the photoionization laser and pulse valve on while the photodissociation laser was off. The S^+ ions images at six different photodissociation wavelengths are shown on the left of Figure 1. The red vertical arrow in the image represents the polarization of the photodissociation laser. No significant effects were observed on the images with the polarization of the photoionization laser changed, indicating that the effects of electron recoil on the parent ions are minor.

All images of different photodissociation wavelengths show a set of concentric rings that correspond to the rovibrational state of the coincident H_2 coproducts. The outer rings correspond to the H_2 ($v = 0$) products with low J. The inner rings correspond to the superimposition of the H_2 ($v = 0$) products with high J and the H_2 ($v = 1$) products with low J. Moreover, as Figure 1(a), 1(b), 1(c), and 1(d) show, the angular distributions are anisotropic. At the same time, the results of Figure 1(e) and 1(f) tend to an isotropic distribution. As the wavelength of the photodissociation laser increases, the intensity of the outmost ring decreases, while the second outmost ring increases. On the other hand, the intensity changes of the inner ring are relatively insignificant.

The total kinetic energy release distributions (TKERs) spectra have been derived (see the Supporting Information) and shown on the right of Figure 1, which can be acquired from individual raw ion images. According to the law of energy conservation in the process of photodissociation

$$E_{int}(H_2) = h\nu - D_0(H_2\text{-}S^+) - E_{TKER} - E_{int}(S^+) \quad (1)$$

where $h\nu$ is the energy of photodissociation laser, $D_0(H_2\text{-}S^+)$ represents the threshold energy for eliminating H_2 from H_2S^+, which was determined by previous work,[24,25] E_{TKER} is the total kinetic energy release of photodissociation products, $E_{int}(H_2)$ is the internal electronic, vibrational, and rotational energy of H_2 products, and $E_{int}(S^+)$ is the energy difference between the S^+ atom products and the ground state $S^+(^4S)$. The rovibrational state distributions of H_2 products in the $S^+(^4S) + H_2(X^1\Sigma_g^+, v, J)$ channel are partially resolved, and two main manifolds are observed, corresponding to the $S^+(^4S) + H_2(X^1\Sigma_g^+, v = 0)$ and the $S^+(^4S) + H_2(X^1\Sigma_g^+, v = 1)$, respectively. Based on the resolved rovibrational structures and the energy conservation law, the total kinetic energy release distributions were fitted using a multipeak fitting method with Gaussian peak profiles.

The feature appears at ~5200 cm^{-1} corresponding to the $H_2(v = 0, J = 0-3)$ products in which the $J = 3$ level is predominantly populated. The peaks appearing at ~4100 cm^{-1} and ~2700 cm^{-1} are assigned to the $H_2(v = 0, J = 5)$ and $H_2(v = 0, J = 7)$, respectively. The weak features below 2000 cm^{-1} belong to the $H_2(v = 1)$ products. Accordingly, we can conclude that the H_2 products are mainly distributed in the vibrational level of $v = 0$ and rotational energy levels with $J < 7$. With the increment of photodissociation wavelength, the distribution of the $H_2(v = 0, J = 5)$ fragments increased, while the distribution of the $H_2(v = 0, J \leq 3)$ fragments decreased. At the photodissociation wavelengths, 336.927, 336.947, and 337.012 nm, the H_2 products are mainly distributed in the vibrational energy level $v = 0$ with the rotational quantum number $J \leq 3$, and the features become weaker with a little increase in wavelengths. In contrast, the $v = 0$, $J = 5$ state for the H_2 products becomes the most populated at 337.059, 337.087, and 337.117 nm.

From the raw ion images, the angular distributions of the photodissociation products for different rovibrational states of $H_2(X^1\Sigma_g^+)$ can be obtained by using

$$I(\theta) = (1/4\pi)[1 + \beta P_2(\cos\theta)] \quad (2)$$

where θ is the crossing angle between the recoil vector of the S^+ cations and the polarization axis of the photodissociation

https://doi.org/10.1021/acs.jpclett.2c01892
J. Phys. Chem. Lett. 2022, 13, 8157−8162

laser, $P_2(\cos\theta) = (3\cos^2\theta\text{-}1)/2$ is the second Legendre polynomial, β is the anisotropy parameter, ranging from −1 to 2 and taking the limiting values of $\beta = 2$ corresponding to a parallel (∥)-type and $\beta = -1$ corresponding to a perpendicular (⊥)-type transition, respectively. The angular distribution curve $I(\theta)$ was acquired by integrating the signal over all product kinetic energies. The β values were obtained by fitting the angular distributions with eq 2 using the least-squares method.

The β values for different rovibrational states of the $H_2(X^1\Sigma_g^+)$ product at the six photodissociation wavelengths are derived and displayed in Figure 2. In the four short wavelengths, 336.927, 336.947, 337.012, and 337.059 nm, the angular distributions are anisotropic with β values around 0.6, suggesting that the dissociation should be fast. On the other side, the results for both longer photodissociation wavelengths, 337.087 and 337.117 nm, show nearly isotropic angular distribution with β values being very close to 0.

Theoretical investigations based on the accurate global full-dimensional PESs were carried out to understand the mechanisms of H_2S^+ photodissociation at the experimental photoexcitation energies. The PESs of $X^2B_1(1^2A'')$, $A^2A_1(1^2A')$, and $1^4A_2(1^4A'')$ states were developed by the FI-NN fitting to a total of 15352 data points calculated with the high-level MRCI-F12+Q/AVQZ in C_s symmetry. Details of PES construction and properties of PESs are given in the Supporting Information.

Figure 3 shows the PESs of $X^2B_1(1^2A'')$, A^2A_1 $(1^2A')$, and $1^4A_2(1^4A'')$ states as functions of the H−H distance and the

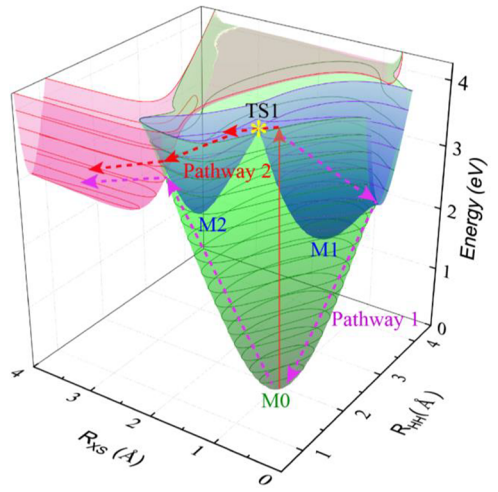

Figure 3. Potential energy surfaces (in eV) for the X $^2B_1(1\ ^2A'')$, A $^2A_1(1\ ^2A'')$, and 1 $^4A_2(1\ ^4A'')$ states of H_2S^+ as a function of the distances R_{HH} and R_{XS}, with the other degree of freedom fully optimized. M0 represents the minimum of the X $^2B_1(1\ ^2A'')$ state; M1 and M2 represent the global minimum and the local minimum of the A $^2A_1(1\ ^2A')$ state, respectively; TS1 represents the first-order saddle point connecting M1 and M2. Two possible pathways are indicated by arrows.

distance between the S atom and the midpoint of the H−H bond, with the other degrees of freedom optimized. The corresponding minimum energy path of $1^2A'$ and the associated energies on $1^2A''$ and $1^4A''$ are shown in Figure 4(a). As shown in Figure 3, once H_2S^+ is photoexcited to the $1^2A'$ state, two possible pathways leading to $H_2 + S^+(^4S)$ from the Franck−Condon region were revealed. Because there exists

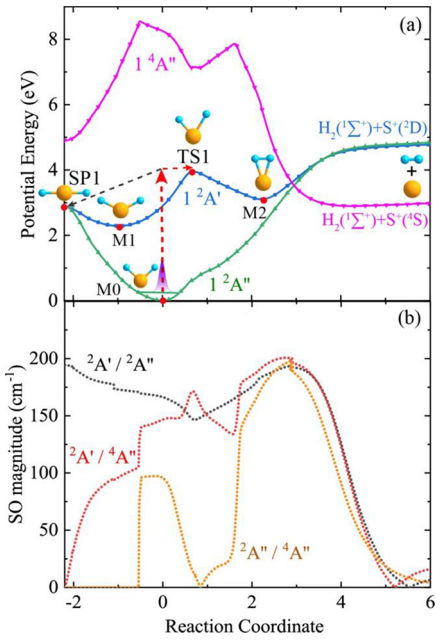

Figure 4. (a) Minimum energy path of the 1 $^2A'$ state and the corresponding energies of 1 $^2A''$ and 1 $^4A''$. The geometries of critical points are indicated. (b) Magnitudes of spin−orbit couplings between 1 $^2A'$/1 $^2A''$, 1 $^2A'$/1 $^4A''$, and 1 $^2A''$ /1 $^4A''$, respectively.

a TS (TS1) connecting two minima (M1 and M2) on the $1^2A'$ state, the dissociation mechanism is sensitive to the photoexcitation energy near the TS energy.

For Pathway 1, the dissociation is initiated by photoexcitation of ground-state H_2S^+ $(1^2A'')$ to the $1^2A'$ state with the energy below TS1, which might then nonadiabatically transit to the ground $1^2A''$ state. The transition from the $1^2A'$ state to the ground $1^2A''$ state can be accessible via both the Renner−Teller coupling around the linear configuration (SP1) and the spin−orbit coupling. The ground-state H_2S^+ $(1^2A'')$ can then transit to the $1^4A''$ state via spin−orbit coupling, finally producing $H_2 + S^+(^4S)$. We can see from Figure 4(a) that the bond angle ∠HSH of H_2S^+ first increases to nearly 180° on $1^2A'$ and then decreases with the evolution on $1^2A''$, and finally the molecule decomposes on $1^4A''$. The computed spin−orbit couplings shown in Figure 4(b) also suggest large values at two crossing regions of $1^2A'/1^2A''$ and $1^2A''/1^4A''$, respectively, indicating the intersystem crossing occurs easily around these regions. Overall, the dissociation via Pathway 1 is a relatively slow process, which evolves on different electronic states, in particular, the $1^2A''$ state with the global minimum of 2.92 eV below the $H_2 + S^+(^4S)$ dissociation limits. This slow and indirect pathway can lead to the isotropic angular distribution of S^+ and β values around 0, as observed by the experiment at the excitation wavelengths of 337.087 and 337.117 nm.

For Pathway 2, on the other hand, the H_2S^+ molecule is photoexcited to the $1^2A'$ state with the energy above TS1, which evolves on $1^2A'$ with two H atoms directly approaching and eventually decomposes into $H_2 + S^+(^4S)$ by intersystem crossing to the repulsive $1^4A''$ state. This direct and fast pathway accounts for the S^+ products with anisotropic angular distributions at four slightly lower photoexcitation energies (336.927 nm−337.059 nm) in Figure 1. The experimentally observed S^+ products with anisotropic angular distributions at shorter photodissociation wavelengths suggest that Pathway 2

https://doi.org/10.1021/acs.jpclett.2c01892
J. Phys. Chem. Lett. 2022, 13, 8157−8162

may dominate the H_2S^+ photodissociation in excitation energy higher than the TS on the $1^2A'$ state. The computed TS energy with zero-point energy correction relative to the ground state minimum is 3.79 eV, which agrees reasonably well with the experimental threshold of about 3.68 eV, determining the transformation of isotropic to anisotropic angular distribution. Theoretically, the potential energies were calculated based on the MRCI(Q)-F12/aug-cc-PVQZ level. The MRCI approach is well-known for the accuracy description of excited states, but its accuracy is certainly not comparable to the gold standard coupled cluster method. Therefore, the energy difference of 0.1 eV between the theoretical and experimental transformation threshold can arise from the MRCI energy errors. The dynamical effects such as tunneling can also contribute to the deviation. Interestingly, it has been found in the study of HCO radical.[33] The H+CO fragments corresponding to different rotational excitations could display different angular distributions which could be related with the state lifetime. Therefore, the specific transition may also play a role together with the photolysis energy, in the dissociation for the H_2S^+. Thus, the observed sensitive variation of angular distributions in a narrow excitation wavelengths region shows unambiguous evidence of two different dissociation mechanisms determined by the transition state on the $1^2A'$ state. These characterizations of potential energy landscapes were also supported by approximate dynamics calculations based on the three adiabatic PESs, as detailed in the Supporting Information.

To summarize, we have investigated the photodissociation dynamics of H_2S^+ near 337 nm in a combined experimental and theoretical study. In a small dissociation laser photon energy range of about 5 cm^{-1}, we have observed significant changes in the product total kinetic energy release distributions and angular distributions. The global full-dimensional PESs were constructed by FI-NN fitting to high-level *ab initio* data points for $1^2A''$, $1^2A'$, and $1^4A''$ states of H_2S^+. The characterization of the PESs reveals two possible dissociation mechanisms near 337 nm relying on the photoexcitation energy, which is sufficient or not to overcome the transition state connecting two minima on the $1^2A'$ state. One is an indirect pathway dominating at an energy below this transition state, in which the H_2S^+ ions first nonadiabatically transit from the $1^2A'$ state to the $1^2A''$ state and eventually dissociate via intersystem crossing to the 1^4A_2 state. The other is a pathway with the energy sufficient to overcome the transition state on $1^2A'$ and directly dissociate by spin−orbit coupling to the repulsive 1^4A_2 state. The two different pathways account for the sensitive variation of angular distributions observed experimentally near 337 nm. The current study shows unambiguous evidence of different photochemistry dynamics controlled by a critical point on the PES in a narrow photoexcitation energy region, which gives valuable insight into the complicated nonadiabatic dynamics.

■ ASSOCIATED CONTENT

Supporting Information

The Supporting Information is available free of charge at https://pubs.acs.org/doi/10.1021/acs.jpclett.2c01892.

Experimental details, product total kinetic energy releases, product branch ratios, and computational details; schematic of experimental apparatus (Figure S1); product branching ratios at six photodissociation wavelengths (Figure S2); optimized geometries of reactant species, product species, and transition states (Figure S3); minimum energy paths (Figure S4); bending potential energy curves (Figure S5); reaction time distributions (Figure S6); product exit angle distributions (Figure S7); product exit angle θ used in current work (Figure S8); comparisons of geometries and adiabatic energies of H_2S^+ (Table S1); and comparisons of vertical energies for H_2S^+ (Table S2) (PDF)

■ AUTHOR INFORMATION

Corresponding Authors

Xiaoguo Zhou − *Department of Chemical Physics, University of Science and Technology of China, Hefei 230026, China;* orcid.org/0000-0002-0264-0146; Email: xzhou@ustc.edu.cn

Bina Fu − *State Key Laboratory of Molecular Reaction Dynamics, Dalian Institute of Chemical Physics, Chinese Academy of Sciences, Dalian 116023, China;* orcid.org/0000-0003-1568-0259; Email: bina@dicp.ac.cn

Xingan Wang − *Department of Chemical Physics, University of Science and Technology of China, Hefei 230026, China;* orcid.org/0000-0002-1206-7021; Email: xawang@ustc.edu.cn

Authors

Zhiwen Luan − *Department of Chemical Physics, University of Science and Technology of China, Hefei 230026, China*

Yanlin Fu − *State Key Laboratory of Molecular Reaction Dynamics, Dalian Institute of Chemical Physics, Chinese Academy of Sciences, Dalian 116023, China*

Yuxin Tan − *Department of Chemical Physics, University of Science and Technology of China, Hefei 230026, China*

Yaling Wang − *Department of Chemical Physics, University of Science and Technology of China, Hefei 230026, China*

Baokun Shan − *Department of Chemical Physics, University of Science and Technology of China, Hefei 230026, China*

Jie Li − *Department of Chemical Physics, University of Science and Technology of China, Hefei 230026, China*

Wentao Chen − *Department of Chemical Physics, University of Science and Technology of China, Hefei 230026, China*

Lijie Liu − *Department of Chemical Physics, University of Science and Technology of China, Hefei 230026, China; State Key Laboratory of Molecular Reaction Dynamics, Dalian Institute of Chemical Physics, Chinese Academy of Sciences, Dalian 116023, China*

Dong H. Zhang − *State Key Laboratory of Molecular Reaction Dynamics, Dalian Institute of Chemical Physics, Chinese Academy of Sciences, Dalian 116023, China;* orcid.org/0000-0001-9426-8822

Xueming Yang − *State Key Laboratory of Molecular Reaction Dynamics, Dalian Institute of Chemical Physics, Chinese Academy of Sciences, Dalian 116023, China; Department of Chemistry, School of Science, Southern University of Science and Technology, Shenzhen 518055, China;* orcid.org/0000-0001-6684-9187

Complete contact information is available at: https://pubs.acs.org/10.1021/acs.jpclett.2c01892

Author Contributions

Z.L. and Y.F. contributed equally to this work.

https://doi.org/10.1021/acs.jpclett.2c01892
J. Phys. Chem. Lett. 2022, 13, 8157−8162

Notes

The authors declare no competing financial interest.

■ ACKNOWLEDGMENTS

This work was supported by the National Key R&D Program of China, (Grant No. 2016YFF0200500), the National Natural Science Foundation of China (Grant Nos. 22125302, 22173099, 22288201, and 21873089), and the LiaoNing Revitalization Talents Program (XLYC1907190). We thank Dr. Anwen Liu, Dr. Kaijun Yuan, and Chang Luo for helpful discussions.

■ REFERENCES

(1) Guo, H.; Yarkony, D. R. Accurate Nonadiabatic Dynamics. *Phys. Chem. Chem. Phys.* **2016**, *18* (38), 26335−26352.
(2) Yuan, K.; Dixon, R. N.; Yang, X. Photochemistry of the Water Molecule: Adiabatic versus Nonadiabatic Dynamics. *Acc. Chem. Res.* **2011**, *44* (5), 369−378.
(3) Oba, Y.; Tomaru, T.; Lamberts, T.; Kouchi, A.; Watanabe, N. An Infrared Measurement of Chemical Desorption from Interstellar Ice Analogues. *Nat. Astrono.* **2018**, *2* (3), 228−232.
(4) Farquhar, J.; Bao, H.; Thiemens, M. Atmospheric Influence of Earth's Earliest Sulfur Cycle. *Science* **2000**, *289* (5480), 756−758.
(5) Zanchet, A.; Lique, F.; Roncero, O.; Goicoechea, J. R.; Bulut, N. J. A. Formation of Interstellar SH^+ from Vibrationally Excited H_2: Quantum Study of $S^+ + H_2 \leftrightarrow SH^+ + H$ Reaction and Inelastic Collision. *Astron. Astrophys.* **2019**, *626*, A103.
(6) Duxbury, G.; Jungen, C.; Rostas, J. Effects of Orbital Angular Momentum in H_2S^+. *Mol. Phys.* **1983**, *48* (4), 719−752.
(7) Karlsson, L.; Mattsson, L.; Jadrny, R.; Bergmark, T.; Siegbahn, K. Vibrational and Vibronic Structure in the Valence Electron Spectrum of H_2S. *Phys. Scr.* **1976**, *13* (4), 229−234.
(8) Barrow, T.; Dixon, R. N.; Duxbury, G. The Renner Effect in a Bent Triatomic Molecule Executing a Large Amplitude Bending Vibration. *Mol. Phys.* **1974**, *27* (5), 1217−1234.
(9) Fiquet-Fayard, F.; Guyon, P. M. Préionisation et Prédissociation dans la Dissociation des Molécules Triatomiques par Impact Électronique. *Mol. Phys.* **1966**, *11* (1), 17−30.
(10) Han, S.; Kang, T. Y.; Kim, S. K. Rotationally Resolved Spectroscopy of the $\tilde{A}\ ^2A_1 \leftarrow \tilde{X}\ ^2B_1$ Transition of H_2S^+ above the Barrier to Linearity Using the Mass-Analyzed Threshold Ionization Photofragment ExcitationTechnique. *J. Chem. Phys.* **2010**, *132* (12), 124304.
(11) Zhao, Y.; Luo, Z.; Chang, Y.; Wu, Y.; Zhang, S. E.; Li, Z.; Ding, H.; Wu, G.; Campbell, J. S.; Hansen, C. S.; et al. Rotational and Nuclear-Spin Level Dependent Photodissociation Dynamics of H_2S. *Nat. Commun.* **2021**, *12* (1), 4459.
(12) Gao, S.; Mo, Y. Ion-Pair Dissociation Dynamics of H_2S in the Photon Energy Range 15.26−15.55 eV. *J. Phys. Chem. A* **2011**, *115* (10), 1781−1786.
(13) Delwiche, J.; Natalis, P. Photoelectron Spectrometry of Hydrogen Sulfide. *Chem. Phys. Lett.* **1970**, *5* (9), 564−566.
(14) Eland, J. H. D. Dissociations of State-Selected $C_2H_2^+$ and D_2S^+ Studied by Photoelectron-Photoion Coincidence Spectroscopy. *Int. J. Mass Spectrom.* **1979**, *31* (1), 161−173.
(15) Möhlmann, G. R.; de Heer, F. J. Lifetimes of the Vibronic $\tilde{A}^2A_1$ States of H_2S^+. *Chem. Phys. Lett.* **1975**, *36* (3), 353−356.
(16) Steadman, J.; Cole, S. K.; Baer, T. Visible and Ultraviolet Resonance Enhance Multiphoton Ionization Photoelectron Spectroscopy of H_2S in the One-Photon Wavelength Region 143−158 nm. *J. Chem. Phys.* **1988**, *89* (9), 5498−5506.
(17) Ashfold, M. N. R.; Bayley, J. M.; Dixon, R. N.; Prince, J. D. Molecular Predissociation Dynamics Revealed through Multiphoton Ionisation Spectroscopy. III. New $^1A_2$ and $^1B_1$ Rydberg States in H_2S and D_2S. *Chem. Phys.* **1985**, *98* (2), 289−313.
(18) Ashfold, M. N. R.; Hartree, W. S.; Salvato, A. V.; Tutcher, B.; Walker, A. A Reinvestigation of the Rydberg States of H_2S and D_2S by Two-Photon Resonant Multiphoton Ionisation Spectroscopy. *J. Chem. Soc. Faraday Trans.* **1990**, *86* (11), 2027−2034.
(19) Baltzer, P.; Karlsson, L.; Lundqvist, M.; Wannberg, B.; Holland, D. M. P.; MacDonald, M. A. An Experimental Study of the Valence Shell Photoelectron Spectrum of Hydrogen Sulphide. *Chem. Phys.* **1995**, *195* (1), 403−422.
(20) Tokue, I.; Yamasaki, K.; Nanbu, S. He* ($2\ ^3S$) Penning Ionization of H_2S. Theoretical Franck-Condon Factors for the $H_2S(\tilde{X}^1A_1,v'=0) \rightarrow H_2S^+(\tilde{X}\ ^2B_1, \tilde{A}\ ^2A_1)$ Ionization and $H_2S^+(\tilde{A}-\tilde{X})$ Transition. *J. Chem. Phys.* **2003**, *119* (12), 5874−5881.
(21) Dixon, R. N.; Duxbury, G.; Horani, M.; Rostas, J. The H_2S^+ Radical Ion. *Mol. Phys.* **1971**, *22* (6), 977−992.
(22) Duxbury, G.; Horani, M.; Rostas, J.; Price, W. C. Rotational Analysis of the Electronic Emission Spectrum of the H_2S^+ Ion Radical. *Proc. Math. Phys. Eng. Sci.* **1972**, *331* (1584), 109−137.
(23) Hochlaf, M.; Weitzel, K. M.; Ng, C. Y. Vacuum Ultraviolet Pulsed-Field Ionization-Photoelectron Study of H_2S in the Energy Range of 10−17 eV. *J. Chem. Phys.* **2004**, *120* (15), 6944−6956.
(24) Webb, A. D.; Dixon, R. N.; Ashfold, M. N. R. Imaging Studies of the Photodissociation of H_2S^+ cations. I. Illustrations of the Role of Nuclear Spin. *J. Chem. Phys.* **2007**, *127* (22), 224307.
(25) Webb, A. D.; Kawanaka, N.; Dixon, R. N.; Ashfold, M. N. R. Imaging Studies of the Photodissociation of H_2S^+ Cations. *II. J. Chem. Phys.* **2007**, *127* (22), 224308.
(26) Duxbury, G.; Jungen, C.; Alijah, A.; Maier, J. P.; Klapstein, D. The Renner−Teller Effect Observed in the Electronic States of H_2S^+. *Mol. Phys.* **2014**, *112* (23), 3072−3084.
(27) Hirsch, G.; Bruna, P. J. Ab initio MRD-CI study on H_2S^+. Dissociation Correlation Diagram for the A^2A1 and B^2B_1 Electronic States. *Int. J. Mass Fnectrom. Ion Phys.* **1980**, *36*, 37−46.
(28) Hirst, D. M. Ab initio Potential-Energy Surfaces for the $\tilde{X}\ ^2B_1$, $\tilde{A}\ ^2A_1$, and $\tilde{B}\ ^2B_2$ States of the H_2S^+ Molecular Ion. *J. Chem. Phys.* **2003**, *118* (20), 9175−9184.
(29) Li, W.-Z.; Huang, M.-B. The $1^2A''$, $1^2A'$, and $2^2A'$ Electronic States of the H_2S^+ Ion Studied Using Multiconfiguration Second-Order Perturbation Theory. *Chem. Phys.* **2005**, *315* (1), 133−141.
(30) Chang, H.-B.; Huang, M.-B. A Theoretical Study on Photodissociation of the A State of the H_2S^+ Ion. *Theor. Chem. Acc.* **2009**, *122* (3), 189−196.
(31) Shao, K.; Chen, J.; Zhao, Z.; Zhang, D. H. Communication: Fitting Potential Energy Surfaces with Fundamental Invariant Neural Network. *J. Chem. Phys.* **2016**, *145* (7), No. 071101.
(32) Chen, R.; Shao, K.; Fu, B.; Zhang, D. H. Fitting Potential Energy Surfaces with Fundamental Invariant Neural Network. II. Generating Fundamental Invariants for Molecular Systems with up to Ten Atoms. *J. Chem. Phys.* **2020**, *152* (20), 204307.
(33) Kable, S. H.; Loison, J. C.; Neyer, D. W.; Houston, P. L.; Burak, I.; Dixon, R. N. Observation of a Parallel Recoil Distribution from a Perpendicular Absorption Transition in Formyl Radicals HCO and DCO. *J. Chem. Phys.* **1991**, *95* (21), 8013−8018.

https://doi.org/10.1021/acs.jpclett.2c01892
J. Phys. Chem. Lett. 2022, 13, 8157−8162